JOC Article
pubs.acs.org/joc

X-ray Diffraction, Solution Structure, and Computational Studies on Derivatives of (3-*sec*-Butyl-2,3-dihydro-1*H*-isoquinolin-4-ylidene)acetic Acid: Compounds with Activity as Calpain Inhibitors

Mercedes Alonso,[†] Roberto Chicharro,[†] Carlos Miranda,[†] Vicente J. Arán,[‡] Miguel A. Maestro,[§] and Bernardo Herradón*[,†]

[†]*Instituto de Química Orgánica General, CSIC, Juan de la Cierva 3, 28006 Madrid, Spain,* [‡]*Instituto de Química Médica, CSIC, Juan de la Cierva 3, 28006 Madrid, Spain, and* [§]*Departamento de Quíimica Fundamental, Facultad de Ciencias, Universidade da Coruña, Campus da Zapateira, 15071 A Coruña, Spain*

herradon@iqog.csic.es

Received September 28, 2009

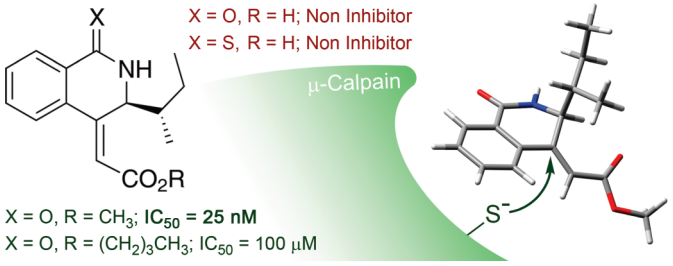

A thorough experimental and computational study of derivatives of (3-*sec*-butyl-2,3-dihydroisoquinolin-4-ylidene)acetic acid was performed. Some of these compounds are calpain inhibitors and could be useful as therapeutic agents, since this enzyme is a Ca^{2+}-dependent cysteine protease involved in a wide variety of metabolic and physiological processes, whose over-activation is associated to several pathological conditions. To gain a better understanding of the structure−activity relationships, a structural analysis was carried out with ^{1}H and ^{13}C NMR spectroscopy and DFT calculations together with the X-ray diffraction data of three compounds. The solid state structures showed that the crystal packing as well as the intermolecular interactions depend on the substituent nature of the COOR group. Also, the reactivity of the exocyclic double bond was theoretically evaluated, finding that the more reactive compound is the most potent inhibitor of calpain (IC_{50} = 25 nM).

Introduction

The design of pharmaceuticals is firmly bound on the availability of a large number of accurate data on biological activity and structure, what allows the structure−activity relationships to be established.[1] In recent years, we have been engaged in the preparation of calpain inhibitors, which is a protease of the CA clan of the cysteine peptidase class.[2] Although the natural substrate of this enzyme has not been unequivocally characterized, it has been found that a wide variety of proteins suffer limited hydrolysis by the catalytic action of calpain.[3] Some of the substrates hydrolyzed by calpain are cytoskeletal proteins, enzymes involved in signal transduction, membrane receptors, and transcription factors; what this means is that calpain can be a key regulatory factor in diverse physiological and metabolic pathways, including apoptosis, cell cycle, neuron plasticity, cell motility, and so on.[4] As a consequence, the over-activation of

(1) (a) *The Practice of Medicinal Chemistry*, 2nd ed.; Wermuth, C. G., Ed.; Elsevier/Academic Press: San Diego, CA, 2003. (b) Nantasenamat, C.; Isarankura-Na-Ayudhya, C.; Naenna, T.; Prachayasittikul, V. *EXCLI J.* **2009**, *8*, 74–88. (c) Salum, L.; Andricopulo, A. *Mol. Diversity* **2009**, *13*, 277–285.

(2) (a) McKerrow, J. H.; Caffrey, C.; Kelly, B.; Loke, P.; Sajid, M. *Annu. Rev. Pathol.: Mech. Dis.* **2006**, *1*, 497–536. (b) Mittl, P. R.; Grütter, M. G. *Curr. Opin. Struct. Biol.* **2006**, *16*, 769–775. (c) Turk, B. *Nat. Rev. Drug Discovery* **2006**, *5*, 785–799. (d) *MEROPS: the peptidase database*. Rawlings, N. D.; Morton, F. R.; Kok, C. Y.; Kong, J.; Barrett, A. J. *Nucleic Acids Res.* **2008**, *36*, D320−325. http://merops.sanger.ac.uk/ (last accessed Sept 24th, 2009).

(3) (a) Friedrich, P. *Biochem. Biophys. Res. Commun.* **2004**, *323*, 1131–1133. (b) Tompa, P.; Buzder-Lantos, P.; Tantos, A.; Farkas, A.; Szilágyi, A.; Bánóczi, Z.; Hudecz, F.; Friedrich, P. *J. Biol. Chem.* **2004**, *279*, 20775–20785. (c) Friedrich, P.; Bozóky, Z. *Biol. Chem.* **2005**, *386*, 609–612.

(4) (a) Goll, D. E.; Thompson, V. F.; Li, H.; Wei, W.; Cong, J. *Physiol. Rev.* **2003**, *83*, 731–801. (b) Jánossy, J.; Ubezio, P.; Apáti, Á.; Magócsi, M.; Tompa, P.; Friedrich, P. *Biochem. Pharmacol.* **2004**, *67*, 1513–1521. (c) Franco, S. J.; Huttenlocher, A. *J. Cell Sci.* **2005**, *118*, 3829–3838. (d) Wu, H.-Y.; Lynch, D. *Mol. Neurobiol.* **2006**, *33*, 215–236. (e) Croall, D.; Ersfeld, K. *Genome Biol.* **2007**, *8*, 218.

Published on Web 12/16/2009 DOI: 10.1021/jo902091u

CHART 1. Generic Structures of Calpain Inhibitors Based on the Isoquinoline (A) and Pyrido[1,2-*b*]isoquinoline (B) Backbones and Their Related Peptide Hybrids (C and D, respectively)

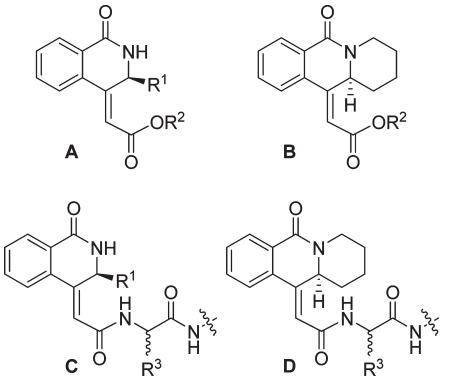

CHART 2. Structures and Biological Activities of the Isoquinolines 1−4 Studied in This Work

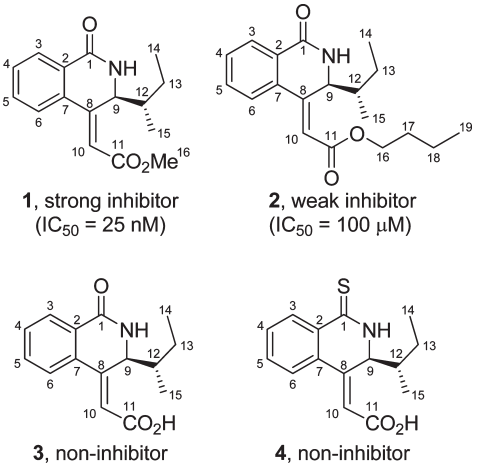

calpain causes an impairment in a diversity of essential biological processes, and, therefore, it is involved in a variety of diseases, including Alzheimer, Parkinson, muscular dystrophy, multiple sclerosis, arthritis, cataract, and other degenerative and aging-related diseases.[5]

Previously, we reported that some partially reduced derivatives of either isoquinoline (**A**) or pyrido[1,2-*b*]isoquinoline (**B**) having an electrophilic olefin were inhibitors of μ-calpain (Chart 1).[6] However, our initial results indicated that the presence of peptidic fragments (e.g., **C** or **D**) was necessary in order to have biological activity.[7] On continuing our structure−activity studies on isoquinoline derivatives, we were delighted to find that the simple isoquinoline derivative **1** (Chart 2) was a strong inhibitor of μ-calpain with an IC_{50} of 25 nM.[8] Some

SCHEME 1[a]

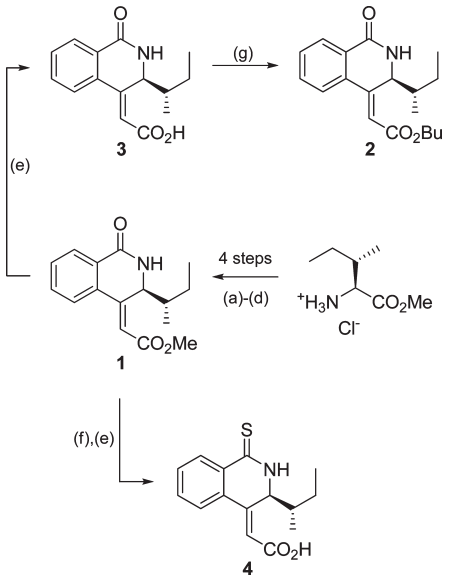

[a]Reagents and conditions: (a) *o*-I-C_6H_4COCl, 1 M K_2CO_3, THF, 0 °C to rt (62% yield); (b) $LiBH_4$, MeOH, THF, −10 °C to rt (85% yield); (c) (i) DMSO/$(COCl)_2$, CH_2Cl_2, Et_3N, −78 °C, (ii) $Ph_3P{=}CHCO_2CH_3$, CH_2Cl_2, −78 °C to rt (80% yield); (d) $Pd(OAc)_2$, Ph_3P, Et_3N, CH_3CN, reflux (77% yield); (e) 1 M LiOH, THF/H2O (96% yield); (f) Lawesson's reagent, toluene, reflux (91% yield); (g) (i) $SOCl_2$, CH_2Cl_2, reflux, (ii) BuOH, CH_2Cl_2, rt (69% yield).

additional advantages of this compound are the following: (1) it has a low molecular weight; (2) it is readily synthesized in multigram scale in a few synthetic operations; and (3) it has a variety of biological activity in cell assays.[9]

To expand our knowledge on the biological activity of methyl (*S*,*S*,*Z*)-(3-*sec*-butyl-1-oxo-2,3-dihydro-1*H*-isoquinolin-4-ylidene)acetate (**1**) we have synthesized closely related compounds to **1**, finding that meanwhile the butyl ester **2** is a weak inhibitor of μ-calpain, and the acid **3** and the thiolactam **4** are noninhibitors (Chart 2).

To deepen on the reasons of the quite different biological activities of these related compounds, we have performed a thorough structural study of **1**−**4**, using experimental (NMR and X-ray diffraction analysis) and computational methodologies.

Results and Discussion

In the following discussion, the numbering of the atoms of molecules **1**−**4** has been homogenized and it is based on the X-ray structures as indicated in Chart 2. The numbering of hydrogen atoms is the same as those atoms to which hydrogens are attached.

Synthesis. The synthesis of **1**−**4** (Scheme 1) has been reported in previous works.[8,10] Compound **1** was obtained as a single stereoisomer and regioisomer by acylation of (*S*,*S*)-isoleucine methyl ester hydrochloride with 2-iodobenzoyl chloride, reduction of the methoxycarbonyl group

(5) (a) Gafni, J.; Ellerby, L. M. *J. Neurosci*. **2002**, *22*, 4842–4849. (b) Zatz, M.; Starling, A. *N. Engl. J. Med*. **2005**, *352*, 2413–2423. (c) Selvakumar, P.; Sharma, R. K. *Int. J. Mol. Med*. **2007**, *19*, 823–827. (d) Azuma, M.; Shearer, T. R. *Surv. Ophthalmol*. **2008**, *53*, 150–163.

(6) For overviews of calpain inhibitors, see: (a) Neffe, A.; Abell, A. *Curr. Opin. Drug Discovery Dev*. **2005**, *8*, 684–700. (b) Carragher, N. O. *Curr. Pharm. Des*. **2006**, *12*, 615–638.

(7) (a) Mann, E.; Chana, A.; Sánchez-Sancho, F.; Puerta, C.; García-Merino, A.; Herradon, B. *Adv. Synth. Catal*. **2002**, *344*, 855–867. (b) Salgado, A.; Mann, E.; Sánchez-Sancho, F.; Herradon, B. *Heterocycles* **2003**, *60*, 57–71.

(8) Chicharro, R.; Alonso, M.; Mazo, M. T.; Arán, V. J.; Herradon, B. *ChemMedChem* **2006**, *1*, 710–714.

(9) Herradon, B.; Chicharro, R.; Arán, V. J.; Alonso, M. PCT Appl. ES2005/070171.

(10) Chicharro, R.; Alonso, M.; Arán, V. J.; Herradon, B. *Tetrahedron Lett*. **2008**, *49*, 2275–2279.

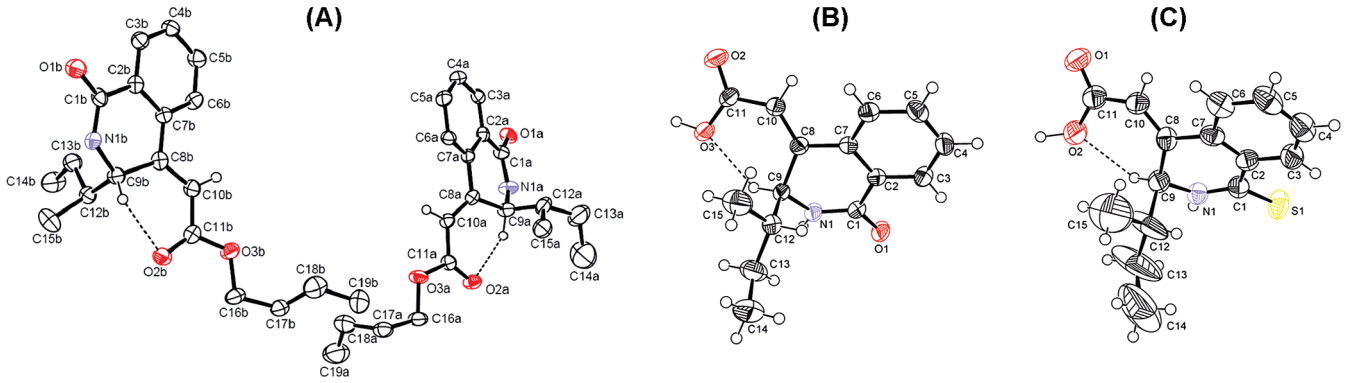

FIGURE 1. Molecular solid state structure of **2** (A, showing the two molecules **2A** and **2B** in the asymmetric unit), **3** (B), and **4** (C) with atom labeling scheme. Displacement ellipsoids are drawn at the 50% probability levels.

with $LiBH_4$, followed by a sequential one-pot Swern−Wittig reaction to give the corresponding *N*-acylated γ-amino-α,β-unsaturated ester, and finally intramolecular cyclization through the Heck reaction. The butyl ester derivative **2** was prepared by hydrolysis of **1** with aqueous LiOH, yielding the corresponding acid **3**, and subsequent reaction of its acid chloride with BuOH. On the other hand, compound **1** was reacted with Lawesson's reagent to give the analogous thiolactam, whose methyl ester group was later hydrolyzed to acid **4** in high overall yield.

Solid State Structures. The solid state structures of compounds **2**−**4** were determined by single-crystal X-ray diffraction and they are presented in Figure 1A−C.[11]

The three compounds crystallize in the noncentrosymmetric *P*2(1)2(1)2(1) space group, so only one enantiomer is present in the crystals. The absolute configuration was assigned as (*S*,*S*) on the basis of the synthetic sequence starting from L-isoleucine. For compound **4**, the *S* configuration was confirmed by the Flack parameter,[12] χ = 0.0(3), based on the anomalous dispersion of the sulfur atom with Mo Kα radiation. Compound **2** crystallizes with two independent molecules in the asymmetric unit, differing mainly in the dihedral angle of the heterocyclic ring and in the disposition of the *sec*-butyl group. The rms deviation between both structures is 0.652 Å excluding hydrogen atoms. Tables S1 and S2 of the Supporting Information show the structural parameters of **2**, **3**, and **4**.

The solid state conformation of the fused bicyclic system is quite similar in the three compounds. As expected, the benzenic rings are planar and aromatic within experimental errors. However, the lactam ring adopts a distorted envelope conformation with an axially oriented *sec*-butyl group: the four sp^2 carbon atoms are coplanar with the benzene ring (allowing the extension of the delocalization of the π-electrons), and the sp^3 one and the pyramidalized nitrogen atom are puckered out of this plane. The deviation of the N1 and C9 atoms from the plane defined by the four sp^2 carbon atoms C1, C2, C7, and C8 is collected in Table S2 of the Supporting Information. It shows that the δ-lactam ring is significantly flatter in **2B**.

A common structural feature to molecules **2**−**4** is that the exocyclic double bond is not in the same plane of the phenyl ring, which, although limiting electron delocalization, avoids steric hindrance due to allylic strain[13] between the olefinic hydrogen H10 and the aromatic hydrogen at C6. Again, the deviation from the coplanarity of the 2,3-dihydro-1*H*-isoquinolin-4-ylidene system is considerably smaller in **2B**. It is interesting to note that the bond length of C8−C7 in **2B** is 0.02 Å shorter than the corresponding length in **2A**. In all of the molecules, it is observed that the carbonyl and thiocarbonyl groups at C1 are noncoplanar with the aromatic ring and this nonplanarity is more accentuated in the thiolactam **4**.

A noteworthy structural difference between molecules **2A** and **2B** and compounds **3** and **4** is the relative disposition of the CO group (C10−C11 conformation) with respect to the double bond. Whereas the carbonyl group adopts an *s-cis* conformation in molecules **2A** and **2B**, it is *s-trans* in compounds **3** and **4** (in the isoquinoline derivatives with a carboxylic group instead of an ester group).[14]

The bulky *sec*-butyl substituent adopts the axial position in all the structures with torsion angles C7−C8−C9−C12 of 75.2−77.3° in **2A**, **3**, and **4**, and of 97.9° in **2B**. Only H12 of the *sec*-butyl group lies directly over the lactam ring in **2A**, **3**, and **4**, whereas both H13a and H13b point toward the lactam ring in **2B**. Therefore, the *sec*-butyl group is rotated about 180° in **2B** [C8−C9−C12−C13 is −176.6° in **2A**, −68.3° in **2B**, 179.78° in **3**, and 174.3° in **4**]. In addition, extended conformations are preferred for ethyl groups in **2B**, **3**, and **4**, showing C9−C12−C13−C14 dihedral angles from 167.2° to 171.8°. Only in **2A**, where this value is −69.5°, is the ethyl chain folded above the isoquinoline moiety.

With respect to the O-*n*-butyl group, while in **2B** the aliphatic chain is fully extended showing a dihedral angle C16−C17−C18−C19 of 176.3°, in **2A** the terminal methyl group is folded with a torsion angle of 77.2°.

(11) Despite attempting additional refinement, a better quality of X-ray diffraction data for compound **4** was not achieved. Nevertheless, the crystallographic data of this compound were good enough to be used as the starting point for DFT calculations.

(12) Flack, H. *Acta Crystallogr., Sect. A: Found. Crystallogr.* **1983**, *39*, 876–881.

(13) (a) Johnson, F. *Chem. Rev.* **1968**, *68*, 375–413. (b) Hoffmann, R. W. *Chem. Rev.* **1989**, *89*, 1841–1860.

(14) A Cambridge Structural Database (CSD) search has been performed with the program ConQuest 1.10 to identify the conformational preferences of C═C—C═O torsion angle in α,β-unsaturated carboxylic acids and esters. Dihedral angle statistics were analyzed with the program Vista (see Figures S1 and S2, Supporting Information). Examination of 260 X-ray structures containing α,β-unsaturated ester moiety led to 271 *s-cis* and 22 *s-trans* conformations (ratio *s-cis*/*s-trans*: 12.3/1), whereas the acid search yielded 133 compounds, finding 107 *s-cis* and 64 *s-trans* conformers (ratio *s-cis*/*s-trans*: 1.67/1).

TABLE 1. HOMA Index Values Calculated for Different Conjugated π-System Moieties of Compounds 2−4

compd	$HOMA_{phenyl}$	$HOMA_{lactam}$	$HOMA_{ext.\ \pi\text{-system}}$
2A	0.974	−0.971	−0.331[a]
2B	0.953	−0.738	0.116[a]
3	0.981	−0.623	−0.048[a]
4	0.868	−0.251	0.056[b]

[a]The extended π-system contains O1, C1, C2, C7, C8, C10, C11, and O2 atoms. [b]The π-system extends over atoms S1, C1, C2, C7, C8, C10, C11, and O1.

The molecular structures of **2**−**4** are stabilized by a nonclassical hydrogen bond (H-bond),[15] C9−H9···O, formed from the carbonyl oxygen of the butyl ester in **2A** and **2B** and from the alcoholic oxygen of the carboxylic group in **3** and **4**. This intramolecular interaction contributes to further stabilize the observed axial configuration of the *sec*-butyl group (see Figure 1).

The structural aromaticity descriptor HOMA (Harmonic Oscillator Model of Aromaticity)[16] has been calculated in order to evaluate the aromaticity of the individual rings of the isoquinoline ring system and the degree of π-electron delocalization between the six adjacent sp^2 carbon (C1, C2, C7, C8, C10, and C11) together with the oxygen/sulfur atoms of the carbonyl/thiocarbonyl groups. HOMA values, calculated from X-ray diffraction data, for the different moieties of compounds **2**−**4** are listed in Table 1. According to HOMA, molecule **2B**, the flattest structure, has the most extended π-electron delocalization.

Although the solid state molecular structures of **2**, **3**, and **4** are quite similar, the different functionalities at the ends of the molecules cause quite different supramolecular packing, reflecting the importance of intermolecular interactions on crystal packing. Whereas **3** and **4** form H-bonds through the O−H of the carboxylic group and N−H of the lactam or thiolactam ring, only **2** can assemble the second kind of H-bonds.

In the crystal structure of **2**, the molecules of **2A** and **2B** are forming a dimer through N−H···O intermolecular H-bonds (Figure 2 and Table 2). According to the graph set theory notation,[17] this dimer is classified as a $R_2^2(8)$ motif. The crystal packing of **2** (Figure 3) shows that the dimers are arranged in antiparallel layers along the *a*-axis, and are maintained by arene−arene interactions.[18] Pairs of phenyl rings of nonequivalent molecules overlap with an interplanar separation of 3.697 Å and a centroid−centroid distance of 3.977 Å in a parallel-displaced orientation. The angle between both rings is 8.9°. The nonequivalent molecules involved in the $\pi-\pi$ stacking interaction are parallel to each other and they are rotated as ca. 77°. Therefore, the alternate

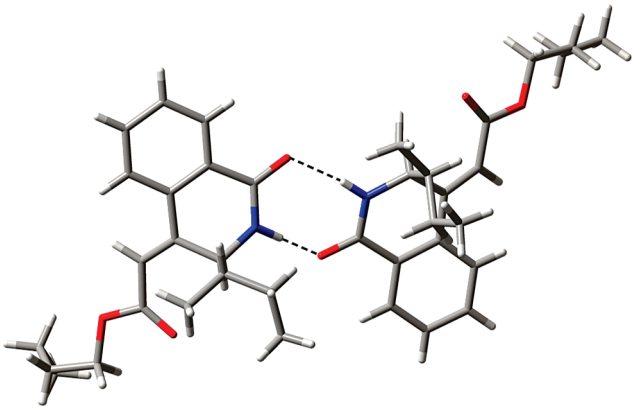

FIGURE 2. Crystal structure of compound **2** showing the dimer formed by two nonequivalent molecules linked by N−H···O hydrogen bonds.

TABLE 2. Potential H-Bonds in the Crystal Structure of 2 and Their Geometries (Å, deg)

D−H···A	d_{D-H}	$d_{H\cdots A}$	$d_{D\cdots A}$	$\angle_{DHA}$	class
N1a−H1a···O1b	0.86	1.94	2.768(4)	160	intermolecular
N1b−H1b···O1a	0.86	2.13	2.971(4)	167	intermolecular
C9a−H9a···O3a	0.98	2.23	2.956(4)	130	intramolecular
C9b−H9b···O2b	0.98	2.26	2.859(4)	118	intramolecular

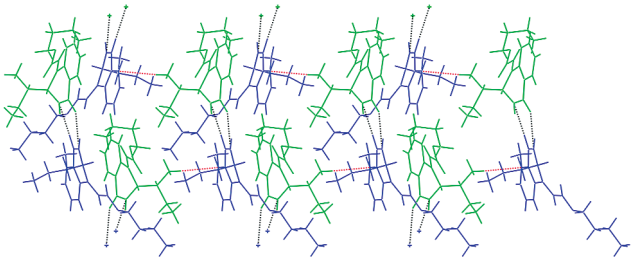

FIGURE 3. View along the *c*-axis of the crystal packing of **2** showing the hydrogen bonds (black dotted line) and the CH···π interactions (red dotted line). Molecules A are indicated in green and B are shown in blue.

arrangement of molecules of **2A** and **2B** along the *a*-axis makes suitable a CH···π interaction between the C15a−H15a group and the phenyl ring of the lower molecule **2B** (H15a···π = 3.302 Å, C15a···π = 3.302 Å, and C15a−H15a···π = 81.8°).[15] A list of geometrical data of putative nonclassic H-bonds of **2** is indicated in Table 2.

The crystal structures of **3** and **4** are quite similar: each molecule of either **3** or **4** is linked to two neighboring molecules through two different H-bonds (Table 3), leading to an infinite chain of molecules along the *b*-axis. Figures 4 and 5 show the two kinds of H-bonds present in the crystal structures of **3** and **4**, respectively: O−H···O/S bonds between the carboxylic group and the carbonyl/thiocarbonyl accepting group of the isoquinoline ring, and N−H···O H-bonds connecting the lactam ring with the carboxylic groups. According to the graph set theory, both can be classified as a chain C(4) motif and their combination generates a new $R_2^2(8)$ pattern. This pattern is quite common in carboxylic acids as noted by Etter[17a] in her insightful analysis of hydrogen bonds in crystal structures. Additionally,

(15) (a) Levitt, M.; Perutz, M. F. *J. Mol. Biol.* **1988**, *201*, 751–754. (b) Umezawa, Y.; Tsuboyama, S.; Takahashi, H.; Uzawa, J.; Nishio, M. *Tetrahedron* **1999**, *55*, 10047–10056. (c) Nishio, M. *CrystEngComm* **2004**, *6*, 130–158. (d) Nishio, M. *Top. Stereochem.* **2006**, *25*, 255–302. (e) Nishio, M.; Umezawa, Y.; Honda, K.; Tsuboyama, S.; Suezawa, H. *CrystEngComm* **2009**, *11*, 1757–1788.

(16) Kruszewski, J.; Krygowski, T. M. *Tetrahedron Lett.* **1972**, *13*, 3839–3842.

(17) (a) Etter, M. C. *Acc. Chem. Res.* **1990**, *23*, 120–126. (b) Bernstein, J.; Davis, R. E.; Shimoni, L.; Chang, N. L. *Angew. Chem., Int. Ed. Engl.* **1995**, *34*, 1555–1573.

(18) (a) Hunter, C. A.; Lawson, K. R.; Perkins, J.; Urch, C. J. *J. Chem. Soc., Perkin Trans. 2* **2001**, 651–669. (b) Hunter, C. A.; Sanders, J. K. M. *J. Am. Chem. Soc.* **2002**, *112*, 5525–5534. (c) Tsuzuki, S. *Struct. Bonding* **2005**, *115*, 149–193.

TABLE 3. Possible H-Bonds in the Crystal Structure of 3 and 4 and Their Geometries (Å, deg)

D−H···A	d_{D-H}	$d_{H\cdots A}$	$d_{D\cdots A}$	$\angle_{DHA}$	class
		3			
O3−H3A···O1[a]	0.97	1.61	2.578(2)	172	intermolecular
N1−H1A···O2[b]	0.86	2.04	2.865(2)	159	intermolecular
C9−H9A···O3	0.98	2.24	2.954(2)	129	intramolecular
C13−H13B···N1	0.97	2.5	2.930(3)	106	intramolecular
		4			
O2−H2A···S1[c]	1.13	2.36	3.195(5)	128	intermolecular
N1−H1A···O1[d]	0.86	2.01	2.865(7)	173	intermolecular
C15−H15A···S1	0.96	2.79	3.390(12)	121	intermolecular
C9−H9A···O3	0.98	2.28	2.969(8)	127	intramolecular
C3−H3···S1	0.93	2.72	3.101(7)	105	intramolecular
C13−H13A···S1	0.97	2.51	2.921(10)	105	intramolecular

[a]Symmetry transformations: $-x$, $y + {}^1/_2$, $-z + {}^3/_2$. [b]Symmetry transformations: $-x$, $y - {}^1/_2$, $-z + {}^3/_2$. [c]Symmetry transformations: $-x+1$, $y - {}^1/_2$, $-z + {}^1/_2$. [d]Symmetry transformations: $-x+1$, $y + {}^1/_2$, $-z + {}^1/_2$. The four molecules of the unit cell of **3** and **4** are related by pseudoinversion center (symmetry) except for the chiral groups.

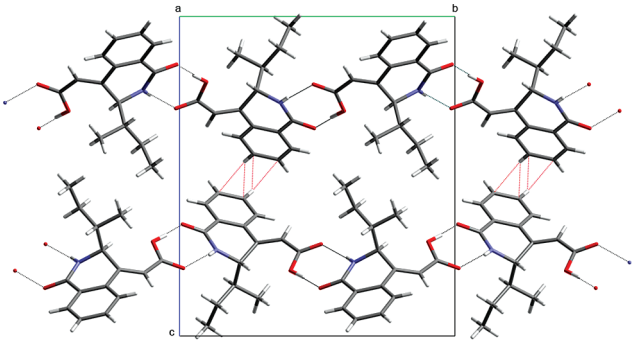

FIGURE 4. View along the *a*-axis of the crystal packing of **3** showing the antiparallel chains of molecules, held by N−H···O intermolecular hydrogen bonds (black contacts). CH···π interactions are represented by red dotted lines.

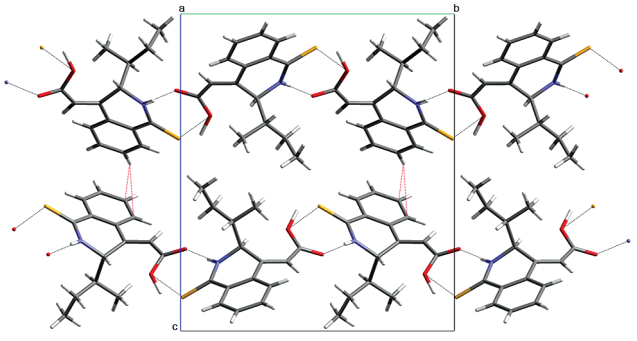

FIGURE 5. View along the *a*-axis of the crystal packing of **4** showing the antiparallel chains of molecules linked by intermolecular hydrogen bonds (black dotted lines). CH···π interactions are indicated by red dotted lines.

a nonclassical weak CH···π H-bond (involving molecules belonging to different and antiparallel chains) is present in the crystal structures of **3** and **4**: a H−C(Ph) bond is nearly perpendicular to the midpoint of a C=C bond in another phenyl ring [H5···C5 = 2.847 Å and C5−H5···C5 = 149.0° (H5···C4 = 2.857 Å and C5−H5···C4 = 167.9°) in **3**; H4···C5 = 3.032 Å and C4−H4···C5 = 157.2° (H5···C6 = 3.095 Å and C5−H5···C4 = 3.928°) in **4**].

As mentioned above, there are also intramolecular H-bonds of the type C−H···X (X = O, N, and S) in the crystal structure of **2**−**4** that assist to stabilize its molecular conformation in the solid state. In **4**, there is an additional intermolecular C15−H15···S interaction between two identical adjacent molecules from different chains in parallel arrangement. The C−H···X interactions that fulfill the geometrical criteria for the existence of H-bonds[19] in the crystal structures of **3** and **4** are indicated in Table 3.

Conformational Studies on 2−4. Experimental and Calculated NMR Spectra in Solution. ^{1}H NMR experiments were carried out in order to determinate the conformation of compounds **2**−**4** in solution. Moreover, the ^{1}H and ^{13}C magnetic shielding tensors of compounds **2**−**4** were computed with the GIAO method[20] in order to compare with the experimental spectral data. The X-ray structures were previously optimized at the B3LYP/6-31G(d) level of theory to refine hydrogen atom positions.

^{1}H NMR experimental chemical shifts of compounds **2**−**4** as well as ^{1}H−^{1}H coupling constants are summarized in Table 4. From the experimental coupling constants $^3J_{H1,H9}$, the H9−C9−N1−H1 dihedral angle can be calculated by using the following Karplus equation:[21]

$$^3J = A\cos^2\varphi - B\cos\varphi + C \qquad (1)$$

As reported elsewhere,[22] there are three different equations to model the vicinal coupling between amide NH and αCH protons with the following parameters (eq 1): $A = 6.7$, $B = 1.3$, $C = 1.5$; $A = 6.4$, $B = 1.4$, $C = 1.9$; and $A = 9.4$, $B = 1.1$, $C = 0.4$. According to these parameters, the range of values has been obtained for the H9−C9−N1−H1 torsion and they are shown in Table 5. These data indicate that the three compounds have nearly the same conformation in the lactam ring with the *sec*-butyl group axially oriented. It is worth noting the close similarity between the values of H9−C9−N1−H1 dihedral angles determined in solution and in the solid state (see Table 5) despite the fact that the accuracy of the position of the hydrogens in the X-ray analysis is not high. It is especially remarkable that this dihedral angle is nearly identical in solution and in molecule **2B** of compound **2**.

Since a good agreement between experimental and theoretical geometrical parameters is found, we can confirm that this level of theory offers a good description of geometries for these kinds of compounds. In fact, the values of the H9−C9−N1−H1 dihedral angle of the optimized structures are much closer to the experimental ones (see Table 5).

(19) The H···X distance is less than the sum of the corresponding van der Waals radii and the C−H···X angle is greater than 100°. (a) Desiraju, G. R.; Steiner, T. *The Weak Hydrogen Bond in Structural Chemistry and Biology*; Oxford University Press/International Union of Crystallography: Oxford, UK, 1999. (b) Jeffrey, G. A. *Crystallogr. Rev.* **2003**, *9*, 135–176. (c) Bialonska, A.; Ciunik, Z. *CrystEngComm* **2006**, *8*, 66–74. (d) Buckingham, A. D.; Del Bene, J. E.; McDowell, S. A. C. *Chem. Phys. Lett.* **2008**, *463*, 1–10.

(20) (a) Cheeseman, J. R.; Trucks, G. W.; Keith, T. A.; Frisch, M. J. *J. Chem. Phys.* **1996**, *104*, 5497–5509. (b) Wolinski, K.; Hinton, J. F.; Pulay, P. *J. Am. Chem. Soc.* **2002**, *112*, 8251–8260.

(21) (a) Ramachandran, G. N.; Chandrasekaran, R.; Kopple, K. D. *Biopolymers* **1971**, *10*, 2113–2131. (b) Demarco, A.; Llinás, M.; Wüthrich, K. *Biopolymers* **1978**, *17*, 637–650. (c) Wüthrich, K.; Billeter, M.; Braun, W. *J. Mol. Biol.* **1984**, *180*, 715–740.

(22) Karolak-Wojciechowska, J.; Czylkowski, R.; Karczmarzyk, Z.; Paluchowska, M. H.; Rys, B.; Szneler, E.; Mokrosz, M. J. *J. Mol. Struct.* **2002**, *612*, 39–47.

TABLE 4. Experimental (δ_{exp}, DMSO-d_6) and Calculated (δ_{calc}) ^{1}H NMR Chemical Shifts (ppm) for 2−4[a]

	2						
		δ_{calc}		3		4	
atom	δ_{exp}	2A	2B	δ_{exp}	δ_{calc}	δ_{exp}	δ_{calc}
H3	7.92[b] dd, 1H	8.22	8.41	7.89[g] dd, 1H	8.33	8.37[i] dd, 1H	8.79
H6	7.80[b] dd, 1H	7.44	7.62	7.72[g] dd, 1H	7.48	7.61 m, 1H	7.41
H4/H5	7.72 m, 2H	7.44	7.37	7.57 m, 2H	7.47	7.61 m, 2H	7.41
H10	6.43 s, 1H	6.16	6.33	6.34 s, 1H	6.09	6.38 s, 1H	6.01
H9	5.20[c] dd, 1H	5.88	5.65	5.24[h] dd, 1H	4.92	5.34[j] dd, 1H	4.90
H12	1.61 m, 1H	1.43	1.46	1.34 m, 1H	1.04	1.37 m, 1H	1.09
H13a	1.37 m, 1H	1.48	1.05	1.46 m, 1H	1.68	1.49 m, 1H	1.71
H13b	1.13 m, 1H	1.08	0.62	1.02 m, 1H	0.70	1.12 m, 1H	0.76
H14	0.75 m, 3H	0.65	0.61	0.74 m, 3H	0.61	0.76[c] t, 3H	0.54
H15	0.75 m, 3H	0.65	0.61	0.74 m, 3H	0.61	0.70[k] d, 3H	0.62
H16	4.13[d] t, 2H	5.58	3.84				
H17	1.61 m, 2H	1.43	1.46				
H18	1.37 m, 2H	1.48	1.05				
H19	0.90[e] t, 3H	0.62	0.74				
NH[a]	6.48[f] br s			8.60[f] d, 1H		11.03 d, 1H	
CO_2H[a]				12.64 br s, 1H		12.77 br s, 1H	
rmsd		0.55	0.30		0.28		0.31

[a]The interchangeable proton signals (NH and CO_2H) were not calculated because δ has a great dependence with the concentration of the sample by the formation of clusters. [b]$J_1 = 7.1$, $J_2 = 1.5$. [c]$J_1 = 7.3$, $J_2 = 4.9$. [d]$J_1 = 6.6$. [e]$J_1 = 7.3$. [f]$J_1 = 4.9$. [g]$J_1 = 7.6$, $J_2 = 1.2$. [h]$J_1 = 7.1$, $J_2 = 4.6$. [i]$J_1 = 7.8$, $J_2 = 1.2$. [j]$J_1 = 8.1$, $J_2 = 4.9$. [k]$J_1 = 6.8$ (^{1}H−^{1}H coupling constants in Hz).

TABLE 5. Experimental and Theoretical H9−C9−N1−H1 Dihedral Angles (in deg) obtained for compounds 2−4

	crystal	solution	theoretical
2A	22.2	36−41	39.4
2B	41.0	36−41	46.0
3	24.25	38−43	37.2
4	24.53	36−41	30.1

Interestingly, the conformer **2B** is more stable than **2A** by 5.3 kJ mol^{-1} ($\Delta G = 5.7$ kJ mol^{-1}).

The calculated and experimental values of the ^{1}H and ^{13}C NMR chemical shifts are collected in Tables 4 and 6, respectively. The qualitative agreement between the calculated and experimental values is very good in all the examined structures: the order of values of the chemical shifts is essentially the same experimentally and computationally (see rmsd values). Only the order of the chemical shifts for C1 and C11 of compound **2** is interchanged.[23] Taking into account

(23) The experimental assignment was based on HMBC correlations: Bax, A.; Summers, M. F. *J. Am. Chem. Soc.* **2002**, *108*, 2093–2094.

TABLE 6. Experimental (δ_{exp}, DMSO-d_6) and Calculated (δ_{calc}) ^{13}C NMR Chemical Shifts (ppm) for 2−4

	2						
		δ_{calc}		3		4	
atom	δ_{exp}	2A	2B	δ_{exp}	δ_{calc}	δ_{exp}	δ_{calc}
C1	165.3	163.0	162.1	162.5	162.8	189.3	197.5
C11	162.4	169.9	169.3	166.7	167.2	166.7	166.9
C8	150.2	161.4	160.9	149.1	159.2	147.9	157.7
C7	134.8	137.7	137.6	135.1	137.8	133.0	133.3
C5	132.7	131.8	132.2	132.6	132.1	131.1	132.6
C4	130.6	130.8	131.3	130.3	131.2	131.0	130.6
C2	128.7	131.9	131.9	128.7	131.1	130.6	131.8
C3	127.1	129.9	130.5	127.0	129.9	130.1	134.4
C6	124.6	124.0	123.0	124.4	124.9	124.4	124.6
C10	116.4	116.7	113.9	117.6	117.7	118.7	117.7
C9	54.2	51.9	59.0	53.9	58.4	55.6	58.7
C12	41.3	40.0	44.8	41.2	43.3	40.3	42.9
C13	24.2	24.0	21.0	24.3	25.3	24.9	26.0
C15	15.1	10.2	11.6	15.0	9.9	14.8	9.6
C14	10.9	2.8	8.4	10.9	8.9	10.9	8.7
C16	63.8	59.8	64.5				
C17	30.2	28.2	30.9				
C18	18.7	20.6	20.6				
C19	13.6	7.5	11.2				
rmsd		4.4	3.9		3.5		4.0

both the size of the isoquinoline derivatives and the high conformational flexibility of the side chains, the overall quantitative agreement expressed by the rmsd is excellent, specially for compound **3**, which proves the efficiency of the computational method. The highest discrepancy between theory and experiment was observed for the C8 atom in all the examined structures, with an error of about 10 ppm.

It is interesting to note that although the experimental chemical shifts of C12 and C13 are closer to the calculated ones for **2A**, the δ_{exp} value for C14 is more similar to δ_{calc} of **2B**, suggesting a preferred *sec*-butyl conformation as in **2A**, where the ethyl group would be fully extended.

These data suggest that the conformation **2B** dominates in solution. On the basis of these results, we can conclude that the conformations of the isoquinoline derivatives **2**−**4** in DMSO solution are quite similar to those found in the solid state.

Conformational Analysis of Methyl (*S*,*S*,*Z*)-(3-*sec*-Butyl-1-oxo-2,3-dihydro-1*H*-isoquinolin-4-ylidene)acetate (1). Because it was not possible to obtain crystals suitable for X-ray diffraction analysis of the isoquinoline **1**, the most potent calpain inhibitor of this series of compounds, we performed its conformational analysis by a combination of molecular dynamics (MD) simulations and DFT calculations. Since the only difference between compounds **1** and **2** concerns the substituent of the ester moiety, the two solid state conformations of derivative **2** were modified and used as starting geometries for MD simulations. In addition, taking into account the results observed in **2**, a third conformation (**1C**) was considered. This conformer is similar to **1A**, but with the *sec*-butyl group totally extended as in **1B**. Three different average structures were obtained and they were further optimized at the B3LYP/6-31G(d) level of theory (Figure 6).

The analysis of the 10-ns MD simulations indicates that the *sec*-butyl group is always in the axial position and, therefore, ring inversion is not observed at 300 K (see the

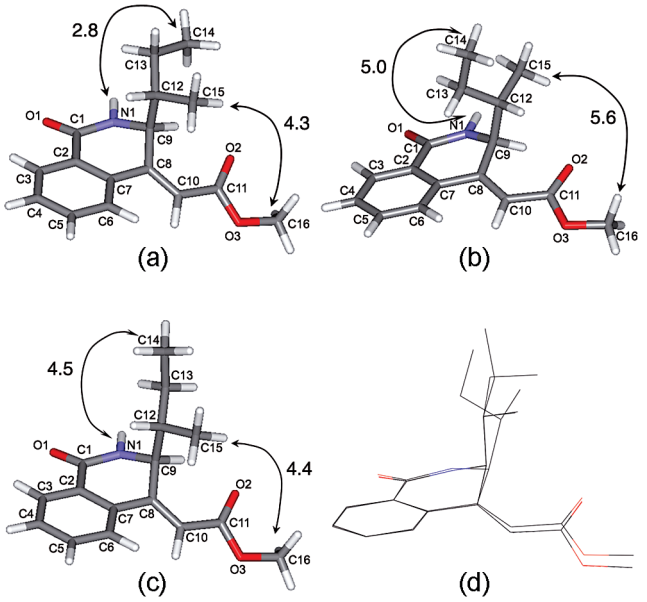

FIGURE 6. Optimized geometries of the three conformers of isoquinoline derivative **1**: (a) **1A**; (b) **1B**; (c) **1C**; and (d) superposition of the three conformations. The theoretical distances between the hydrogen atoms in which NOEs were observed are shown.

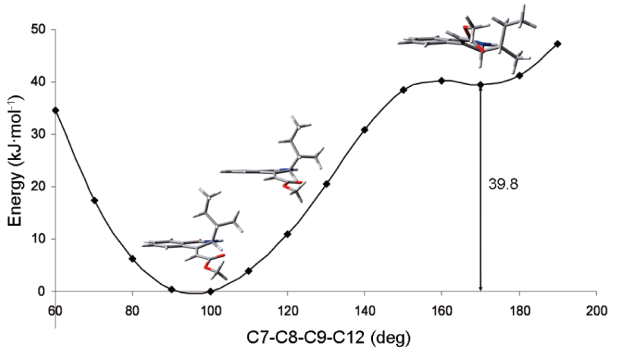

FIGURE 7. Plot of relative energy vs. C7−C8−C9−C12 dihedral angle of compound **2**.

Supporting Information, Table S3). In fact, the calculated energy barrier for the ring inversion of methyl ester **1** is 39.8 kJ·mol^{-1} (Figure 7). Furthermore, the exocyclic double bond is never coplanar with the phenyl ring along the MD trajectories of all conformers, and thus, the less crowded face of the electrophilic double bond is easily accessible for a nucleophilic attack. A remarkable fact is that both the initial structures of **1A** and **1B** converged to **1C**, and all the conformations underwent free rotation around the single bond of the α,*β*-unsaturated ester system prevailing (more than 90%) the *s-cis* configurations. Figure 8 shows a graphic representation of the selected dihedral angles involved in conformational exchange along MD trajectories. Similarly to compound **2**, the flattest conformation **1B** is more stable than **1A** by 2.1 kJ mol^{-1} (ΔG = 3.3 kJ mol^{-1}).

^{1}H NMR and NOE experiments provide evidence that the conformation of compound **1** in solution is quite similar to the proposed ones. Thus, on one hand the range of values obtained for the H9−C9−N1−H1 dihedral angle ($^3J_{H1,H9}$) is 33−40°, being closer to the torsion of −40° present in conformer **1A** (Supporting Information, Table S4). On the

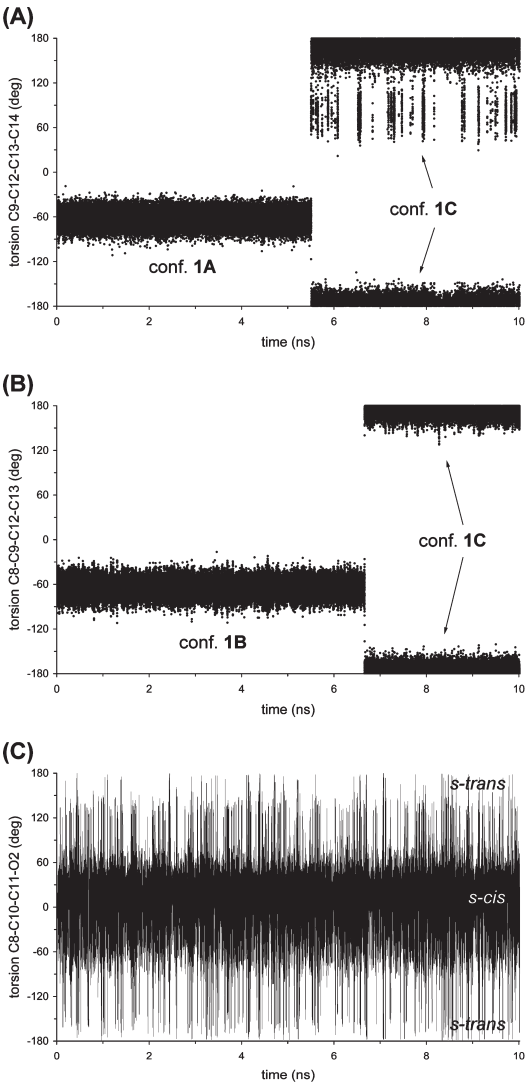

FIGURE 8. (A) C9−C12−C13−C14 dihedral angle of **1A** and (B) C8−C9−C12−C13 dihedral angle of **1B** plotted against time to illustrate their interconversion to **1C** along MD simulations in DMSO. (C) Time-dependent variation of the C8−C10−C11−C12 torsion angle of **1C** showing the fast *s-cis*/*s-trans* equilibria.

other hand, qualitative NOE experiments (DMSO-d_6) revealed a strong enhancement between the olefinic proton H10 and the aromatic protons, confirming the presence of the *Z* isomer in solution. Further weaker NOE enhancements were observed between the protons attached to the methyl group C15 and the methyl ester, and between the amidic proton and the methyl group of the ethyl moiety, respectively. These NOE enhancements are consistent with a major conformer **1A**, in which the corresponding methyl groups are pointing at the methyl ester and at the NH, respectively. In conformer **1B**, the distances between these protons exceed 4.5 Å.

The experimental and calculated values of the ^{1}H and ^{13}C NMR chemical shifts of the three conformers are summarized in Table 7. A visual inspection of the data reveals that the experimental ^{1}H and ^{13}C chemical shifts are consistent with those calculated theoretically. As previously observed with **2**−**4**, only the order of the chemical shifts for C1 and C11 of compound **1** is interchanged. The rmsd between the

TABLE 7. Experimental δ_{exp} and Calculated δ_{calc} ^{1}H and ^{13}C NMR Chemical Shifts (ppm) of Conformers 1A, 1B, and 1C

		δ_{calc}		
atom	δ_{exp}	**1A**	**1B**	**1C**
		^{1}H NMR		
H3	7.92[a] dd, 1H	8.33	8.37	8.31
H6	7.81[a] dd, 1H	7.46	7.52	7.41
H4/H5	7.62 m, 2H	7.41	7.42	7.42
H10	6.43 s, 1H	6.17	6.32	6.23
H9	5.19[b] dd, 1H	5.96	5.63	5.62
H16	3.71 s, 3H	3.43	3.45	3.44
H12/H13	1.62 m, 3H	1.40	1.01	1.18
H15/H14	0.75 m, 6H	0.67	0.63	0.61
rmsd		0.37	0.35	0.33
		^{13}C NMR		
C1	165.6	162.6	161.9	162.4
C11	162.5	170.4	169.7	170.4
C8	150.6	161.5	161.4	161.6
C7	134.8	137.7	137.3	138.0
C5	132.7	132.0	132.0	131.9
C4	130.6	130.8	132.0	131.4
C2	128.8	131.2	131.7	131.5
C3	127.1	129.8	130.5	129.9
C6	124.5	124.0	122.6	124.0
C10	115.9	115.9	113.3	117.1
C9	54.3	51.4	59.3	56.2
C16	51.4	48.8	48.8	48.8
C12	41.4	39.8	45.1	43.5
C13	24.2	23.8	21.1	24.9
C15	15.0	10.2	11.3	9.0
C14	10.8	2.8	8.6	8.9
rmsd		4.46	4.28	4.25

[a] J_1 = 7.08 Hz, J_2 = 1.46 Hz. [b] J_1 = 7.08 Hz, J_2 = 5.13 Hz.

experimental and calculated chemical shifts is very similar for all the conformers. While the experimental NMR signals for H9 and H10 are more similar to the estimated values of conformers **1B** and **1C**, the *sec*-butyl moiety corresponds better with a conformation type **1A**. Furthermore, regarding ^{13}C NMR chemicals shifts, the lowest rmsd value is found for **1C** where δ_{calc} for C14 is quite similar to δ_{calc} for **1B**.

All these data seem to support that the preferred conformation is **1C**, which is quite similar to **1A** but with an extended conformation of the ethyl moiety of the *sec*-butyl group. DFT calculations on **1C** indicate that this conformation is more stable than **1B** and **1A** with small energy differences of 0.42 and 2.5 kJ mol^{-1}, respectively.

Since the starting geometries of **1** were built by modification of solid state structures of **2**, the three conformations obtained for compound **1** are also *s-cis*. To evaluate the relative stability of the *s-trans* and the *s-cis* rotamers, we have optimized the *s-trans* conformer of **1**. According to the calculations, the *s-cis* conformer is around 13 kJ mol^{-1} more stable than the *s-trans* in all studied conformations. Even though the *cisoid*−*transoid* conformational equilibrium is observed along the MD trajectories of **1A**−**C**, the *s-trans* configurations are only detected below 10% of the time (Table S3). These data suggest that the *s-cis* rotamer is the major one at equilibrium in solution for the esters of (3-*sec*-butyl-1-oxo-2,3-dihydro-1*H*-isoquinolin-4-ylidene)-acetic acid.

Computational Support to the Biological Activity. A common mechanism for the inactivation of cysteine protease is through the reaction of the SH-group of the cysteine residue with an electrophilic functionality of the inhibitor.[24] μ-Calpain is a particular cysteine protease whose distinctive feature is the activation by Ca^{2+}.[25] Despite this different mechanism of activation, it is well-known that the active site of calpain is a pocket located in the major subunit with an active cysteine residue, quite similar to papaine and other related cysteine proteases. Therefore, the inhibition of calpain by **1** and related compounds is likely through the reaction with the SH-group of the cysteine residue of the active center of calpain.[26] The high activity of **1** as a calpain inhibitor must arise from two facts: on one side, a suitable recognition pattern by the active site of the enzyme,[27] and on the other hand, an adequate reactivity of the electrophilic functionality of the inhibitor.

The bond-forming step involves movement of electrons from the HOMO of the nucleophile to the LUMO of the unsaturated carbonyl compound. Thus, the inhibitory activity of these Michael acceptors must correlate with the electron affinities (*A*) of the electrophilic double bond. The higher *A*, the more reactive the Michael acceptor, and consequently a greater inhibition capacity could be expected. Figure 9 shows the LUMO surfaces of compounds **1**−**4**. The shape of the LUMO orbital is very similar in the four molecules, even though the coefficients of the atomic orbital vary from esters **1** and **2** to acids **3** and **4** (Table 8). In the case of esters **1** and **2**, the largest LUMO coefficient is at the β-carbon of the α,β-unsaturated system (C8), suggesting that the nucleophilic attack is directed toward this atom. It is noteworthy that the highest coefficient at C8 is obtained for isoquinoline derivative **1**.

Electron affinities were computed at the B3LYP/6-31++G(d,p) level of theory, since this method has been demonstrated to be accurate in reproducing experimental *A* values with an error of less than 0.1 eV.[28] Furthermore, with the aim to explain the differences observed in the

(24) (a) Berti, P. J.; Storer, A. C. *J. Mol. Biol.* **1995**, *246*, 273–283. (b) Otto, H.-H.; Schirmeister, T. *Chem. Rev.* **1997**, *97*, 133–172. (c) Leung-Toung, R.; Li, W.; Tam, T. F.; Kaarimian, K. *Curr. Med. Chem.* **2002**, *9*, 979–1002. (d) Schirmeister, T.; Kaeppler, U. *Mini Rev. Med. Chem.* **2003**, *3*, 361–373. (e) Santos, M. M. M.; Moreira, R. *Mini Rev. Med. Chem.* **2007**, *7*, 1040–1050.

(25) (a) Bozóky, Z.; Alexa, A.; Tompa, P.; Friedrich, P. *Biochem. J.* **2005**, *388*, 741–744. (b) Croall, D. E.; Vanhooser, L. M.; Cashon, R. E. *Biochim. Biophys. Acta* **2008**, *1784*, 1676–1686. (c) Toke, O.; Bánóczi, Z.; Tárkányi, G.; Friedrich, P.; Hudecz, F. *J. Pept. Sci.* **2009**, *15*, 404–410. (d) This mechanistic feature of activation is unique between protease, and it has been advantageously used to design nonelectrophilic calpain inhibitors, see: Montero, A.; Mann, E.; Chana, A.; Herradon, B. *Chem. Biodiversity* **2004**, *1*, 442–457. (e) Montero, A.; Albericio, F.; Royo, M.; Herradon, B. *Org. Lett.* **2004**, *6*, 4089–4092, and references cited therein (f) Although the electrophilicity of the conjugate double bonds in the carboxylates is expected to be lower than that in the corresponding esters, we evaluated both kinds of compounds as calpain inhibitors since they can act through the nonelectrophilic mechanism indicated above.

(26) Kunakbaeva, Z.; Carrasco, R.; Rozas, I. *THEOCHEM* **2003**, *626*, 209–216, and references cited therein

(27) (a) Hubbard, S. J.; Thornton, J. M.; Campbell, S. F. *Faraday Discuss.* **1992**, *93*, 13–23. (b) Tyndall, J. D. A.; Nall, T.; Fairlie, D. P. *Chem. Rev.* **2005**, *105*, 973–1000.

(28) Baranovski, V. I.; Denisova, A. S.; Kuklo, L. I. *THEOCHEM* **2006**, *759*, 111–115.

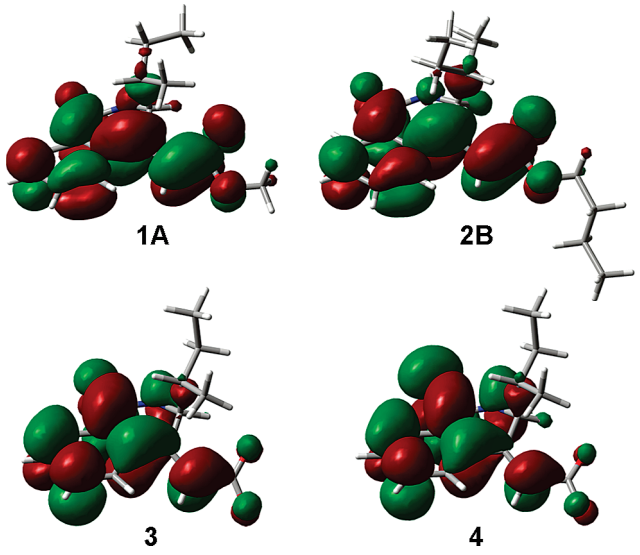

FIGURE 9. LUMO orbital of compounds **1** (conformer A), **2** (conformer B), and carboxylates of **3** and **4**.

TABLE 8. Calculated LUMO Coefficients for the Atoms of the α,β-Unsaturated Carboxylic System for Derivatives 1−2 and Carboxylates of 3−4

compd	C_8	C_{10}	C_{11}	O_2[a]	O_3[b]
1A	0.2990	−0.2426	−0.2188	0.2033	0.1468
1B	−0.2812	0.2333	0.2020	−0.1989	−0.1382
1C	0.2875	−0.2364	−0.2143	0.2001	0.1434
2A	−0.2862	0.2380	0.2134	−0.2014	−0.1444
2B	−0.2753	0.2313	0.1971	−0.1950	−0.1359
3	−0.0731	0.1923	0.0362	−0.0671	−0.0808
4	−0.1189	0.1827	0.0925	−0.0749	−0.1038

[a] O_1 in compound **4**. [b] O_2 in compound **4**.

TABLE 9. B3LYP/6-31++G(d,p) Reactivity Descriptors (values in eV) for Derivatives 1−2 and Carboxylates 3−4

compd	ε_{HOMO}	ε_{LUMO}	$\Delta E_{LUMO-HOMO}$	A	I	μ	η	ω
1A	−6.85	−2.36	4.49	0.854	8.362	−4.608	3.754	2.828
1B	−6.74	−2.42	4.32	0.914	8.250	−4.582	3.668	2.862
1C	−6.88	−2.36	4.51	0.855	8.388	−4.621	3.767	2.835
2A	−6.83	−2.32	4.51	0.841	8.313	−4.577	3.736	2.803
2B	−6.72	−2.39	4.33	0.905	8.199	−4.552	3.647	2.841
3	−2.17	1.18	3.35	−2.422	4.186	−0.882	3.304	0.118
4	−2.36	0.61	2.97	−2.021	4.222	−1.101	3.121	0.194

biological activity, other electronic properties, apart from the electron affinities, such as HOMO and LUMO orbital energies (ε_{HOMO} and ε_{LUMO}), the energy difference between frontier orbitals ($\Delta E_{HOMO-LUMO}$), as well as global reactivity indices (chemical potential, μ; chemical hardness, η; and electrophilicity index, ω) derived from DFT have been calculated (Table 9).[29] Taking into account that carboxylic acids **3** and **4** are deprotonated at pH values of the experimental assays, the electronic properties have been calculated from their corresponding carboxylates. Electron affinity (A) and ionization potential (I) calculations were carried out from the geometry of the neutral system, calculating the electronic energies of the corresponding cation and anion.

The three conformations of methyl ester (**1A**−**C**) and the two of butyl ester (**2A**,**B**) have positive values of A, being the electron affinity values of **1** are slightly higher than those of **2**. So, these compounds react favorably with the cysteine residue of the calpain active site. Likewise, the electrophilic index (ω), a property that measures the capability of a molecule to accept electrons, is higher in the isoquinoline derivative **1**. Since the electron affinity and electrophilic index of **1** are higher, its inhibitory activity must be greater. On the other hand, carboxylates **3** and **4** have highly negative A values and small ω values, which explain the inactivity toward calpain of these carboxylic acids or other derivatives containing a carboxylic group close to the α,β-unsaturated system.

Conclusions

A comprehensive structural analysis on derivatives of (3-*sec*-butyl-2,3-dihydro-1*H*-isoquinolin-4-ylidene)acetic acid has been performed with experimental (NMR and X-ray diffraction) and computational methods. The results have shown differences between ester and acid derivatives in both molecular structure and crystal packing, these differences steming from different functionalities present in the molecules (amides, thioamides, ester, carboxylic acids, arene, C−H donating groups) able to participate in a variety of intermolecular interactions. Since these structural features have been frequently used as components of tectons,[30] the experimental results can be useful in the field of crystal engineering.[31] While the molecules of ester **2** are arranged in dimers by means of H-bonds, acids **3** and **4** are organized in antiparallel chains. The conformational analysis and theoretical study of the most potent calpain inhibitor **1** have confirmed, apart from the dynamic mobility among conformers, that the *sec*-butyl group in the axial position freezes the ring inversion in these isoquinoline derivatives, leaving accessible the less crowded face of the exocyclic double bond. Moreover, we have further demonstrated a structure−activity relationship for the calpain inhibition, based on the reactivity of the double bond of this kind of compounds with the SH-group of the cysteine residue of the calpain active site. The acidic compounds **3** and **4** are noninhibitors since at physiological pH the negative charge of the carboxylate group prevents the approach of the sulfur anion. In addition, the highest inhibitory activity of the ester derivatives is related to both the shape of the LUMO orbital and the highest values of electron affinity and electrophilic index. In summary, the theoretical calculations model with high accuracy the experimental results and we have proved that the COOR group is a fundamental factor for inhibiting calpain in isoquinoline derivatives.

Experimental Section

Crystal Structure Analysis of Derivatives of (3-*sec*-Butyl-2,3-dihydro-1*H*-isoquinolin-4-ylidene)acetic Acid. Suitable single

(29) For additional information about the theoretical background of the reactivity indices see: Alonso, M.; Casado, S; Miranda, C.; Tarazona, J. V.; Navas, J. M.; Herradon, B. *Chem. Res. Toxicol.* **2008**, *21*, 643–658.

(30) Hosseini, M. W. *Acc. Chem. Res.* **2005**, *38*, 313–323.

(31) (a) Moulton, B.; Zaworotko, M. J. *Chem. Rev.* **2001**, *101*, 1629–1658. (b) Braga, D. *J. Chem. Soc., Chem. Commun.* **2003**, 2751–2754. (c) Price, S. L.; Price, L. S. *Struct. Bonding* **2005**, *115*, 81–123. (d) Desiraju, G. R. *Angew. Chem., Int. Ed.* **2007**, *46*, 8342–8356.

crystals of either **2**, or **3**, or **4** were obtained at room temperature by slow diffusion of methanolic solutions of the corresponding derivative. Data collection for X-ray analysis was obtained with use of an area detector single-crystal diffractometer with graphite monochromated Mo Kα radiation (λ = 0.71073 Å) operating at 50 kV and 30 mA. Data were collected over a ϕ and ω scans hemisphere of the reciprocal space by a combination of the number of frames of intensity sets. Each frame covered 0.3° in ω and the first 50 frames were recollected at the end of data collection to monitor crystal decay. Absorption corrections were applied with the SADABS program.[32] The structures were solved with the SHELXTL-PC software[33] by direct methods and refined by full-matrix least-squares methods on F^2. Treatment of hydrogen atoms was mixed, located in density maps and included in calculated positions, and refined in the riding mode. The details of the data collection and structure refinement are summarized in Table S5 of the Supporting Information. The structure drawings were prepared with the programs MERCURY[34] and ORTEP-3.[35] The absolute configurations at the stereogenic centers were assigned according to the synthetic schemes that start from amino acids of known stereochemistry.

The structure of compound **2** was determined by single-crystal X-ray diffraction at 100 and 298 K. At room temperature, due to the higher conformational flexibility of the aliphatic chains, the molecular structure presents certain disorder in the atomic positions of the *sec*-butyl group as well as in the butyl ester of both molecules **2A** and **2B**.

NMR Measurements. Chemical shifts (δ) are reported in parts per million and the coupling constants are indicated in hertz. The ^{1}H and ^{13}C NMR spectra data were recorded in 2 mM DMSO-d_6 solutions. ^{1}H NMR spectra were referenced to the chemical shift of either TMS (δ = 0.00 ppm) or the residual proton in the deuterated solvent. ^{13}C NMR spectra were referenced to the chemical shift of the deuterated solvent. NOESY spectra were acquired by using the standard pulse sequence.

Computational Details. DFT calculations were performed with the Gaussian-03 suite of programs.[36] Full geometry optimizations of compounds **1**−**4** were performed at the B3LYP/6-31G* level of theory.[37−39] Vibrational frequency calculations at the same level of theory confirmed that all structures were minima on the potential energy surface. For compounds **2**−**4**, the starting geometries for the calculations were those obtained in the X-ray diffraction analysis. In the case of **2**, the two different conformations (**2A** and **2B**) found in the crystallographic unit cell were considered. On the other hand, the starting geometry for the quantum-chemical calculation of **1** was obtained from the molecular dynamics (MD) simulations, using MMFF94 force field[40] and model charges as implemented in Sybyl, version 7.0.[41] The MD simulations were performed at constant temperature (300 K) by coupling the system to a thermal bath, using the Berendsen algorithm with a coupling constant of 100 fs. The simulations were carried out in a vacuum (with a distance-dependent dielectric constant ε = 1) for 10 ns, using a time step of 1 fs, leaving 20 ps to equilibrate the system. As the starting conformation, we used analogues of both molecular solid state structures of compound **2**, replacing the butyl ester by a methyl ester and subsequently minimizing. Additionally, the inversion barrier energy for the lactam ring was estimated at the B3LYP/6-31G(d) level of theory for compound **1** by changing the C7−C8−C9−C12 dihedral angle by 10° steps, from 60° to 120°.

The ^{1}H and ^{13}C magnetic shielding tensors of the B3LYP/6-31G*-optimized structures were computed with the Gauge-Independent Atomic Orbital (GIAO) method at the B3LYP/6-311+G(2d,p) level.[20] To compare isotropic shieldings with the experimentally observed chemical shifts, the NMR parameters for TMS were calculated at the same level and used as the reference molecule. For compound **1**, the shielding computations were also performed at the RHF/6-311+G(2d,p) level of theory, finding a worse correlation with the experimental data and a larger computational time.

The HOMA values were calculated for both the solid state molecular structures and the DFT-optimized geometries, using eq 2:[16,42]

$$\mathrm{HOMA} = 1 - \frac{\alpha}{n}\sum_{i=1}^{n}(R_{\mathrm{opt}} - R_i)^2 \qquad (2)$$

where n is the number of atoms taken into the summation, and α is an empirical constant fixed to give HOMA = 0 for a model nonaromatic system and HOMA = 1 for a system with all bonds equal to an optimal value R_{opt}, assumed to be realized for a fully aromatic system. R_i is the running bond length.

Finally, the electron affinity (A), ionization potential (I), as well as the global reactivity descriptors have been calculated at the B3LYP/6-311G(d,p) level of theory, since this method has been demonstrated to be accurate in reproducing experimental A values with an error of less than 0.1 eV.[43] The theoretical basis for the reactivity descriptors has been amply developed elsewhere.[44] I and A are determined from the electronic energies of the systems having $N-1$, N, and $N+1$ electrons at the geometry of the neutral system. Using I and A, the chemical potential (μ), the chemical hardness (η), and the global electrophilic index (ω) were calculated according to eqs 3−5, respectively.

$$\mu \approx -\frac{(I+A)}{2} \qquad (3)$$

(32) Sheldrick, G. M. *SADABS*, Program for Absorption Corrections Using Bruker CCC Detectors, University of Göttingen, Göttingen, Germany, 1986.
(33) Sheldrick, G. M. *SHELXTL-PC*, Program for Crystal Structure Solution, University of Göttingen, Göttingen, Germany, 1997.
(34) *MERCURY*, CSD 2.0, New Features for the Visualization and Investigation of Crystal Structures; Macrae, C. F.; Bruno, I. J.; Chisholm, J. A.; Edgington, P. R.; McCabe, P.; Pidcock, E.; Rodriguez-Monge, L.; Taylor, R.; van de Streek, J.; Wood, P. A. *J. Appl. Crystallogr.* **2008**, *41*, 466−470. Web address: http://www.ccdc.cam.ac.uk/prods/mercury/.
(35) *ORTEP-3*, for Windows; Farrugia, L. J. *J. Appl. Crystallogr.* **1997**, *30*, 565−566. Web address: http://www.chem.gla.ac.uk/~louis/software/ortep3/.
(36) Frisch, M. J.; Trucks, G. W.; Schlegel, H. B.; Scuseria, G. E.; Robb, M. A.; Cheeseman, J. R.; Montgomery, J. A., Jr.; Vreven, T.; Kudin, K. N.; Burant, J. C.; Millam, J. M.; Iyengar, S. S.; Tomasi, J.; Barone, V.; Mennucci, B.; Cossi, M.; Scalmani, G.; Rega, N.; Petersson, G. A.; Nakatsuji, H.; Hada, M.; Ehara, M.; Toyota, K.; Fukuda, R.; Hasegawa, J.; Ishida, M.; Nakajima, T.; Honda, Y.; Kitao, O.; Nakai, H.; Klene, M.; Li, X.; Knox, J. E.; Hratchian, H. P.; Cross, J. B.; Adamo, C.; Jaramillo, J.; Gomperts, R.; Stratmann, R. E.; Yazyev, O.; Austin, A. J.; Cammi, R.; Pomelli, C.; Ochterski, J. W.; Ayala, P. Y.; Morokuma, K.; Voth, G. A.; Salvador, P.; Dannenberg, J. J.; Zakrzewski, V. G.; Dapprich, S.; Daniels, A. D.; Strain, M. C.; Farkas, O.; Malick, D. K.; Rabuck, A. D.; Raghavachari, K.; Foresman, J. B.; Ortiz, J. V.; Cui, Q.; Baboul, A. G.; Clifford, S.; Cioslowski, J.; Stefanov, B. B.; Liu, G.; Liashenko, A.; Piskorz, P.; Komaromi, I.; Martin, R. L.; Fox, D. J.; Keith, T.; Al-Laham, M. A.; Peng, C. Y.; Nanayakkara, A.; Challacombe, M.; Gill, P. M. W.; Johnson, B.; Chen, W.; Wong, M. W.; Gonzalez, C.; Pople, J. A. *Gaussian 03*, revision B.04; Gaussian, Inc., Pittsburgh, PA, 2003.
(37) Becke, A. D. *Phys. Rev. A* **1988**, *38*, 3098–3100.
(38) Becke, A. D. *J. Chem. Phys.* **1993**, *98*, 1372–1377.
(39) Lee, C. T.; Yang, W. T.; Parr, R. G. *Phys. Rev. B* **1988**, *37*, 785–789.
(40) (a) Halgren, T. A. *J. Comput. Chem.* **1996**, *17*, 490–641. (b) Halgren, T. A. *J. Comput. Chem.* **1999**, *20*, 720–748.
(41) *Sybyl molecular modeling system*; Tripos Associated, St. Louis, MO.
(42) Krygowski, T. M. *J. Chem. Inf. Comput. Sci.* **1993**, *33*, 70–78.
(43) Baranovski, V. I.; Denisova, A. S.; Kuklo, L. I. *THEOCHEM* **2006**, *759*, 111–115.
(44) Geerlings, P.; De Proft, F.; Langenaeker, W. *Chem. Rev.* **2003**, *103*, 1793–1874.

$$\eta \approx \frac{(I-A)}{2} \tag{4}$$

$$\omega = \frac{\mu^2}{2\eta} = \frac{(I+A)^2}{4(I-A)} \tag{5}$$

Acknowledgment. Taken in part from the Ph.D. theses of M.A and R.C. We thank the Spanish Ministry of Education and Science (Projects CTQ2004-01978 and CTQ2007-64891/BQU) for financial support and the Centro de Supercomputación de Galicia (CESGA) for the use of the Compaq HPC 320 supercomputer. M.A. thanks the Spanish Ministry of Education and Science for a FPU fellowship. C.M. thanks the Spanish National Research Council for a JAE-Doc contract. We also thank Mr. Iván Escabias for technical assistance.

Supporting Information Available: Structural parameters of **2**, **3**, and **4** (Tables S1 ans S2), lowest, highest and average values of dihedral angles involved in the conformational exchange of **1A**−**1C** (Table S3), selected dihedral angles for conformers **1A**, **1B**, and **1C** calculated at B3LYP/6- 31G* (Table S4), and crystal data and structure refinement for **2**−**4** (Table S5); histogram showing the distribution of C=C—C=O torsion angles (Figures S1 and S2), characterization data, and copies of ^{1}H and ^{13}C NMR spectra of compounds **1**−**4**; X-ray crystallographic files (CIF) for derivatives **2**−**4**; and computational data. This material is available free of charge via the Internet at http://pubs.acs.org. The CIF files are also available from the Cambridge Crystallographic Data Centre, 12 Union Road, Cambridge, CB2 1EZ, U.K. [fax: +44(0) 1223 336033 or e-mail deposit@ccdc.cam.ac.uk], under CCDC reference nos. 748814 (**2**), 748815 (**3**), and 748816 (**4**).